

Mechanically driven interface propagation in biological tissues

Jonas Ranft^{1,2}, Maryam Aliee², Jacques Prost³, Frank Jülicher² and Jean-François Joanny¹

¹ Institut Curie, UMR 168 (CNRS, UPMC Univ Paris 6), 26 rue d'Ulm, F-75005 Paris, France

² Max-Planck-Institut für Physik komplexer Systeme, Nöthnitzer Str. 38, D-01187 Dresden, Germany

³ ESPCI ParisTech, 10 rue Vauquelin, F-75005 Paris, France

E-mail: julicher@pks.mpg.de and jean-francois.joanny@curie.fr

Received 20 September 2013, revised 27 January 2014

Accepted for publication 28 January 2014

Published 5 March 2014

New Journal of Physics **16** (2014) 035002

doi:[10.1088/1367-2630/16/3/035002](https://doi.org/10.1088/1367-2630/16/3/035002)

Abstract

Many biological tissues consist of more than one cell type. We study the dynamics of an interface between two different cell populations as it occurs during the growth of a tumor in a healthy host tissue. Recent work suggests that the rates of cell division and cell death are under mechanical control, characterized by a homeostatic pressure. The difference in the homeostatic pressures of two cell types drives the propagation of the interface, corresponding to the invasion of one cell type into the other. We derive a front propagation equation that takes into account the coupling between cell number balance and tissue mechanics. We show that in addition to pulled fronts, pushed-front solutions occur as a result of convection driven by mechanics.

Keywords: tissue dynamics, growth, front propagation, cell competition

1. Introduction

Animal tissues are made of many different cell types, and interfaces between different cell populations are ubiquitous in the developing and adult organism [1]. An example is the interface that forms between a growing tumor and the healthy cells of the surrounding host tissue [2].



Content from this work may be used under the terms of the [Creative Commons Attribution 3.0 licence](https://creativecommons.org/licenses/by/3.0/). Any further distribution of this work must maintain attribution to the author(s) and the title of the work, journal citation and DOI.

In this article, we study how such interfaces between two distinct cell populations evolve in the presence of cell division and cell death, focussing on the effects of mechanical coupling between the net cell division rates and pressure. It has been hypothesized that the rates of cell division and apoptosis (cell death) are not only dependent on the biochemical conditions present in the tissue but depend on mechanical forces exerted by the surrounding cells [3, 4]. This suggestion was recently underpinned by experimental findings that demonstrate the variation of the net cell division rate with an externally applied pressure [5]. Here, we develop a continuum theory of two cell populations separated by an interface. Our theory takes into account rates of cell division and death which can be influenced by local stress. Resulting cell flows and interface movements follow from the dynamics of cells coupled to force balance in the tissue, and we find moving front solutions that describe the invasion of one tissue into a second one.

2. Tissue hydrodynamics

To investigate the dynamics of tissues with two distinct cell populations, we develop a continuum description that accounts for cell flow fields and stress distributions on large scales. We assume that the tissue comprises cells of type A and B with number densities $n_{A,B}$ and average cell volumes $\Omega_{A,B}$, respectively, such that $n_A\Omega_A + n_B\Omega_B = 1$. Cell number balance is expressed by

$$\partial_t n_i + \partial_\alpha (n_i v_\alpha^i) = n_i k_i, \quad (1)$$

where v_α^i is the velocity of the cell flow field of type i ($i = A, B$), and $k_i = k_d^i - k_a^i$ is the respective net cell division rate, i.e., the difference between the rates of cell division and apoptosis. The rates k_i in general depend on pressure. Their variation is characterized by the homeostatic pressures P_i^h : the homeostatic pressure P_i^h of a tissue is the value of the pressure P for which the tissue is in a homeostatic state in which cell division and apoptosis balance and no net growth occurs. Near the homeostatic state, one can expand the net cell division rate to linear order in pressure differences as $k_i \simeq \kappa_i (P_i^h - P)$. Here, κ_i is a coefficient that in principle is different for the two cell types A and B . For simplicity, we choose the same value $\kappa_i = \kappa$ for the two tissues in the following and investigate the effects of a finite difference of the homeostatic pressures between the two tissues $\Delta P^h \equiv P_A^h - P_B^h > 0$.

Some tissues are separated from each other by physical barriers such as the basal membrane [6]. However, tissue interfaces may also be smooth with possible mixing of cells of different types, see figure 1. On large scales, the shape of the interface is then described by the volume fraction $\phi \equiv n_A\Omega_A$ as a function of position. The average cell velocity v_α is given by

$$v_\alpha = \phi v_\alpha^A + (1 - \phi) v_\alpha^B, \quad (2)$$

and the relative flux J_α obeys

$$\phi v_\alpha^A = \phi v_\alpha + J_\alpha, \quad (1 - \phi) v_\alpha^B = (1 - \phi) v_\alpha - J_\alpha. \quad (3)$$

Under the assumption that the cells are incompressible, i.e., Ω_A and Ω_B constant, the cell number balance equations for each cell type then combine to a condition on the average velocity v_α and a dynamic equation for ϕ ,

$$\partial_\alpha v_\alpha = \phi k_A + (1 - \phi) k_B, \quad (4)$$

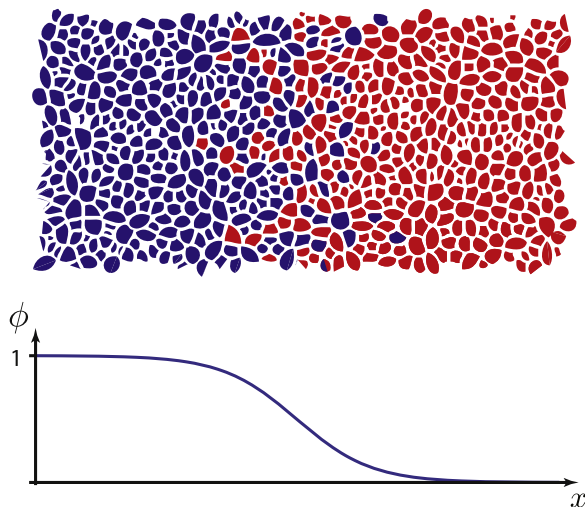


Figure 1. Smooth interface between cells of different type. In the presence of cell diffusion the two populations mix near the interface, which gives rise to a smooth interfacial profile of the volume fraction ϕ of the blue cells as a function of position x .

$$\partial_t \phi + v_\alpha \partial_\alpha \phi = -\partial_\alpha J_\alpha + \phi(1 - \phi)(k_A - k_B). \quad (5)$$

Equation (4) generalizes the the classical incompressibility condition on the divergence of the velocity in the presence of cell division.

In a previous work, we have shown that cell division and apoptosis give rise to a diffusive motion of cells even in the absence of spontaneous cell motility [7]. The existence of such an effective diffusion requires the presence of noise in the tissue, for example due to cell shape fluctuations and to the stochasticity of cell division and apoptosis. Such processes can give rise to mutual diffusion between the two cell types that can be described by an effective diffusion coefficient D and generates a relative flux $J_\alpha = -D\partial_\alpha \phi$. Note that the effective diffusion constant is not caused by thermal fluctuations.

Taking the dependence of cell proliferation on pressure into account, the dynamic equation for ϕ then becomes

$$\partial_t \phi + v_\alpha \partial_\alpha \phi = D\partial_\alpha^2 \phi + \phi(1 - \phi)\kappa\Delta P^h. \quad (6)$$

Equation (6) is a generalized version of the Fisher–Kolmogorov equation which was initially put forward to describe the expansion dynamics of advantageous alleles in a population with shared genome [8, 9]. However, the dynamics of the cell volume fraction described by equation (6) contains an additional term that describes advection with velocity v_α . This velocity is generated in the tissue by active processes and is related to the proliferation of the two cell populations via equation (4). This is a situation that is very different from cases where flows are created externally such as in studies of bacterial colony growth as e.g. in [10]. Since the net cell division rates depend on pressure, the Fisher population dynamics is eventually coupled to the tissue mechanics. This coupling is generic for tissues, where cells do not only divide and die but also interact mechanically. To our knowledge, diffusive growth has so far been discussed without mechanical interactions [11].

To solve for the velocity field v_α , we need to consider the stress distributions and force balance in the tissue. In the absence of external forces, force balance is expressed by $\partial_\beta \sigma_{\alpha\beta} = 0$,

where $\sigma_{\alpha\beta}$ denotes the stress tensor in the tissue. The stress tensor can be split into an isotropic and a traceless part as $\sigma_{\alpha\beta} = -P\delta_{\alpha\beta} + \tilde{\sigma}_{\alpha\beta}$, where P is the total pressure and $\tilde{\sigma}_{\alpha\alpha} = 0$. For an incompressible tissue, P becomes a Lagrange multiplier to impose the generalized incompressibility constraint and from equation (4) we find

$$P = P_B^h + \phi\Delta P^h - (\partial_\alpha v_\alpha)/\kappa. \quad (7)$$

In the hydrodynamic limit, the deviatoric stress $\tilde{\sigma}_{\alpha\beta}$ is given by the constitutive equation

$$\tilde{\sigma}_{\alpha\beta} = 2\eta\tilde{v}_{\alpha\beta} - B\left[(\partial_\alpha\phi)(\partial_\beta\phi) - \frac{1}{3}(\partial_\gamma\phi)(\partial_\gamma\phi)\delta_{\alpha\beta}\right], \quad (8)$$

where we assumed that the tissue behaves as a viscous fluid on long times [7, 12]. Here, η is the shear viscosity and $\tilde{v}_{\alpha\beta} = \frac{1}{2}(\partial_\alpha v_\beta + \partial_\beta v_\alpha - \frac{2}{3}\partial_\gamma v_\gamma\delta_{\alpha\beta})$ is the traceless part of the velocity gradient tensor. The second term on the right-hand side is due to the coupling between stress and composition gradients and its form is dictated by symmetry. It corresponds to the Ericksen stress in systems near thermodynamic equilibrium, and it can be derived explicitly from a Landau–Ginzburg free energy depending on a scalar parameter ϕ [13]. If the width of the interface is of order l , the surface tension between A and B cells is of order B/l . It describes interfacial tensions as they arise for example from differential adhesion between the two cell types [12].

3. Interface propagation dynamics

We are interested in the propagation of an interface between two cell populations that are at their respective homeostatic states and at rest at $x = \pm\infty$. We consider a thin, effectively two-dimensional tissue of fixed height h subject to friction with the underlying substrate [14], which breaks Galilean invariance. Note that for bulk, i.e. three-dimensional, tissues, the role of substrate friction could be played by friction with the interstitial fluid. This can be discussed in descriptions of tissues with permeation [15].

Force balance in the film reads

$$\partial_\beta \bar{\sigma}_{\alpha\beta} = \gamma v_\alpha \quad (9)$$

($\alpha, \beta = x, y$), where γ is a coefficient describing friction with the substrate and $\bar{\sigma}_{\alpha\beta}$ is the stress in the film averaged in the z -direction

$$\bar{\sigma}_{\alpha\beta} = \frac{1}{h} \int_0^h \sigma_{\alpha\beta} dz. \quad (10)$$

For simplicity, we consider tissues for which ϕ is homogeneous along y and fields vary with x only. From the force balance equation (9), using the expressions for P and $\tilde{\sigma}_{\alpha\beta}$, we obtain an equation for the velocity profile v_x ,

$$\left(\kappa^{-1} + \frac{4}{3}\eta\right)\partial_x^2 v_x - \Delta P^h \partial_x \phi - \frac{2}{3}B\partial_x^2 \phi \partial_x \phi = \gamma v_x. \quad (11)$$

Equations (6) and (11) define the dynamics of interface propagation, together with the boundary conditions $\phi(-\infty) = 1$, $\phi(+\infty) = 0$, and $v_x(\pm\infty) = 0$. These equations can be written in a dimensionless form,

$$\partial_T \phi + V \partial_x \phi = \partial_x^2 \phi + \phi(1 - \phi), \quad (12)$$

$$\Lambda^2 \partial_x^2 V - V = 2\Lambda V_0 \partial_x \phi (1 + \beta \partial_x^2 \phi). \quad (13)$$

Here, we have used the characteristic interface width l_0 and timescale t_0 with

$$l_0 = (D/(\Delta P^h \kappa))^{1/2}, \quad t_0 = 1/(\Delta P^h \kappa), \quad (14)$$

to normalize lengths and times: $X = x/l_0$, $T = t/t_0$, and $V = v_x t_0/l_0$. We have furthermore introduced the dimensionless parameters

$$\Lambda^2 = \left(1 + \frac{4}{3} \kappa \eta\right) \Delta P^h / (D\gamma), \quad V_0 = \Delta P^h / (2D\gamma\Lambda), \quad \beta = \frac{2}{3} B\kappa / D.$$

For $V_0 = 0$, the convective velocity vanishes, $V = 0$. Starting with a steep initial condition $\phi(X) = (1 + e^{X/\epsilon})^{-1}$, with $\epsilon \leq 1$, the system reaches for long times traveling-wave solutions of the form $\phi(X, T) = \Phi(U)$, where $U = X - CT$ with wave speed $C = C_0$ and interface profiles $\Phi(U) = \Phi_0(U)$ where $C_0 = 2$ [16, 17]. This solution of the classical Fisher equation is a so-called pulled-front solution for which the wave speed is determined by the linearized dynamics in the tail of the profile. Pulled-front solutions cannot have larger wave speeds than $C = 2$. Here we ask whether traveling-wave solutions persist when $V_0 > 0$ and tissue mechanics and advection have to be taken into account. A simple limit occurs when $\Lambda \gg 1$. In this case, equations (12) and (13) decouple because $V(U=0) \simeq V_0$ remains approximately constant along the interface where $\phi(X)$ varies. From this argument, we find for $\beta = 0$ that $V \partial_x \phi \simeq V_0 \partial_x \phi$ in equation (12). Thus, the interface profile is again given by Φ_0 , however with traveling speed $C = C_0 + V_0$. Finite interfacial tension due to $\beta > 0$ does not change this result as long as $\beta \ll \Lambda$. Such solutions are so-called pushed-front solutions for which the wave speed is determined by nonlinearities as discussed below [17].

We obtain numerical solutions to the dynamic equations (12) and (13) for different values of V_0 , Λ , and β . Starting from a steep initial interface, the interface evolves to a stationary profile $\Phi(U)$ and moves with a speed C for all tested parameter values. Examples of traveling-wave profiles $\phi(U)$ and $V(U)$ are shown in figure 2. For small V_0 as well as for $\Lambda \gg 1$, the profiles are well captured by the approximate solution Φ_0 to the original Fisher equation. Deviations start to be important for larger values of V_0 and finite interfacial-tension coefficient β , see figure 2(g): because of the term $\propto \partial_x^2 \phi$ in equation (13), the interfacial profile broadens, and wave speed increases. The dimensionless wave speed C is shown in figure 3 for different values of V_0 , Λ , and β . Our numerical analysis confirms the simple Fisher-wave limit for $\Lambda \gg 1$, in which the advective velocity V_0 adds up to the wave speed C_0 . It is interesting to note the effect of finite β on the observed wave speeds. For $\beta = 0$, the wave speed C is bounded from above by $C_0 + V_0$, and C increases with increasing Λ towards the predicted value $C_0 + V_0$. For large enough β , the reverse can be observed: for finite Λ , the wave speed C actually exceeds $C_0 + V_0$ and decreases with Λ for fixed V_0 . Taken together, these results highlight the role of the interplay between cellular diffusion, cell–substrate friction, and the mechanical coupling of cell proliferation to pressure.

One can distinguish between pulled fronts and pushed fronts [17]. The velocity of pulled fronts is set by the dynamics of the asymptotic tail which pulls the main profile behind. Because the tail decays to zero, its dynamics can be understood by a linearized theory. Pushed fronts are

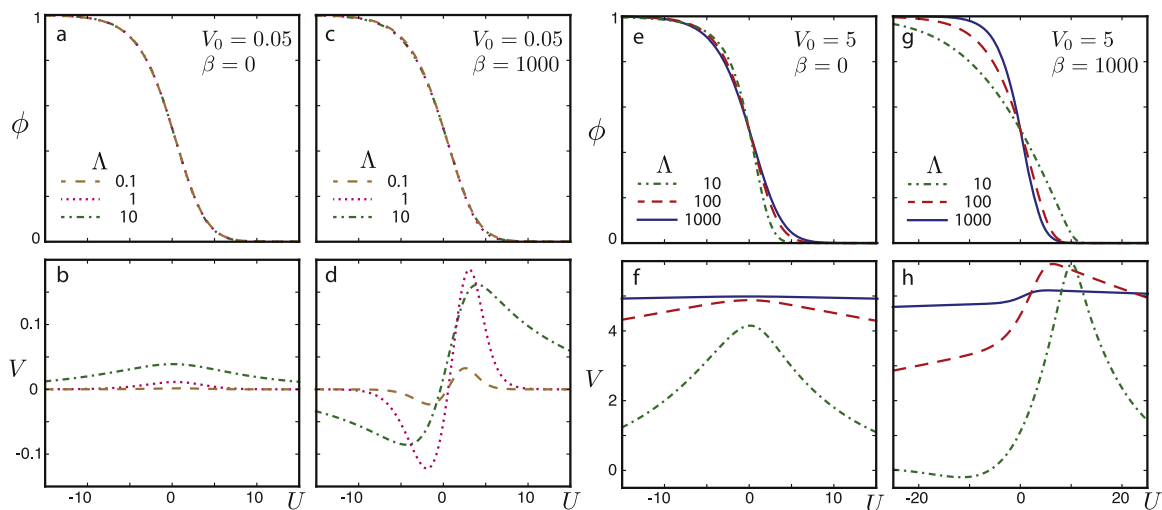


Figure 2. Interface profile ϕ and dimensionless cell velocity V for different driving force V_0 and for different values of Λ as indicated in the absence of interfacial tension, $\beta = 0$, (left panels, (a)–(d)) and for $\beta = 10^3$ (right panels, (e)–(h)). Both $\phi(X, T) = \Phi(U)$ and $V(X, T) = V(U)$ are shown as functions of the coordinate $U = X - CT$; note also the change of scale in panels (g), (h). The values of V_0 are indicated.

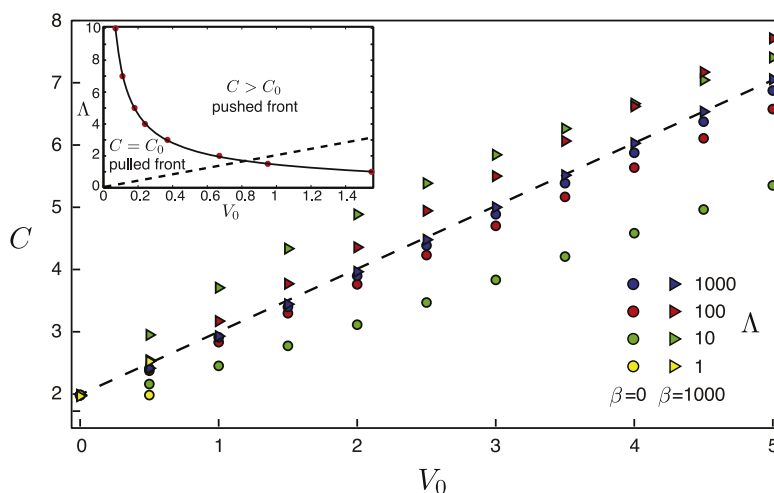


Figure 3. Dimensionless wave speed C of traveling waves for varying driving amplitude V_0 and different values of Λ in the absence of interfacial tension, $\beta = 0$ (circles), and for $\beta = 10^3$ (triangles). The approximation $C = C_0 + V_0$ is plotted as a dashed black line, see text for details. The inset shows the phase diagram of traveling waves in terms of dimensionless parameters Λ and V_0 , when $\beta = 0$. The red dots are the measured transition points between the pushed and pulled fronts. The black line is an interpolation of these data points. The parameter values below the dashed line in the inset, where $V_0 < \Lambda/2$, are unphysical as they cannot be reached in our model.

driven by the part of the profile where nonlinearities are essential. The profile pushes the linear tail forward at a speed that is larger than the pulled-front velocity. Both pulled- and pushed-front solutions can be obtained as profiles $\phi(U)$ and $V(U)$ that solve equations (12) and (13). Such solutions exist for all $C > 0$. The tails of the corresponding profiles are of the form $\phi(U) \simeq d_1 e^{-\lambda_1 U} + d_2 e^{-\lambda_2 U}$ which follows from linearizing equations (12) and (13). Here, d_1 and d_2 are coefficients and the (inverse) decay lengths are given by $\lambda_{1,2} = C/2 \mp [(C/2)^2 - 1]^{1/2}$, with $\lambda_1 \leq \lambda_2$. For localized initial conditions, the system either reaches a pulled-front solution with $C = C_0 = 2$ and $\lambda_{1,2} = 1$ or a pushed-front solution for which $C > C_0$. In the latter case, the velocity C is set by the requirement that the coefficient $d_1 = 0$ must vanish such that the asymptotic behavior of the front is given by $\phi(U) \simeq d_2 e^{-\lambda_2 U}$, corresponding to the steeper front.

This analysis allows us to distinguish pulled-front solutions from pushed fronts in our numerical study. The inset of figure 3 shows a line separating two regions in which pulled and pushed fronts occur as a function of V_0 and Λ , in the case where $\beta = 0$. For small V_0 front propagation is dominated by diffusion and the system develops a pulled front which moves at the same dimensionless speed $C = C_0$ as a Fisher wave without advection. Beyond a critical value of V_0 , the front is pushed by nonlinearities and moves at an increased speed C that depends on V_0 in this advection-dominated regime. Both regimes are separated by a sharp transition from pulled to pushed fronts shown as a solid line.

4. Tissue invasion in circular geometry

The case of a linear geometry discussed above has been chosen for conceptual clarity. For a small clone of A cells surrounded by B cells on a substrate, the expansion is more realistically captured by a growing circular domain of A cells in two dimensions. Using circular symmetry for simplicity, the dynamic equation for the cell volume fraction ϕ reads in polar coordinates

$$\partial_t \phi + v_r \partial_r \phi = D \left(\partial_r^2 \phi + \frac{\partial_r \phi}{r} \right) + \phi(1 - \phi) \kappa \Delta P^h, \quad (15)$$

where r is the radial coordinate. The force balance reads

$$\left(\kappa^{-1} + \frac{4}{3} \eta \right) \left[\partial_r^2 v_r + \frac{\partial_r v_r}{r} - \frac{v_r}{r^2} \right] - \gamma v_r = \Delta P^h \partial_r \phi + \frac{2}{3} B \left(\partial_r^2 \phi + \frac{\partial_r \phi}{r} \right) \partial_r \phi. \quad (16)$$

The boundary conditions are given by $\phi'(0) = 0$, $\phi(\infty) = 0$, $v_r'(0) = 0$, and $v_r(\infty) = 0$. Note that traveling waves of the form $\phi(r, t) = \Phi(r - ct)$ cannot exist for this system because the dynamic equations are not invariant with respect to changes of r . In the limit of long times, however, the radius of the interface becomes large, $r_i \gg \max(l_0, \Lambda l_0)$, and one approaches the one-dimensional case described above. For smaller r_i , the finite curvature of the interface has to be taken into account.

We obtain numerical solutions to the dynamic equations, starting from localized initial conditions. The resulting behavior is shown in figure 4, where an initially localized distribution of A cells first decreases in magnitude and widens before it increases its magnitude and grows out radially. Interestingly, the number of A cells first decreases, because of the increased pressure due to the interfacial tension, which counteracts the proliferative advantage of the stronger A cells (see inset in figure 4). The time dependence of the total number of A cells

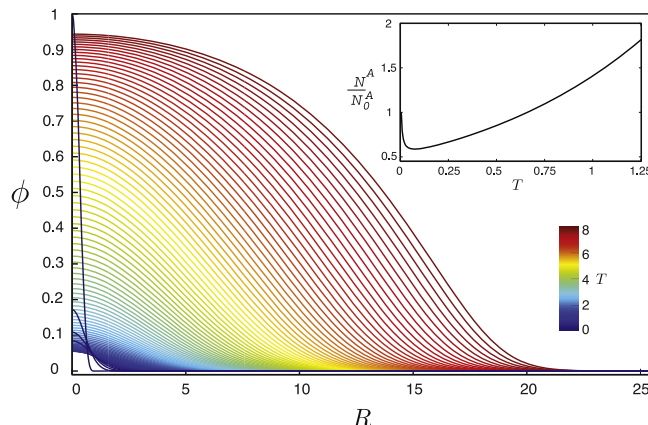


Figure 4. Time-evolution of the interface shape between two cell populations in the cylindrical geometry. The profile of the volume fraction ϕ is plotted as a function of normalized radius $R = r/l_0$ for different dimensionless times T shown by a color code. We start from an initially localized distribution of A cells with higher homeostatic pressure surrounded by B cells of lower homeostatic pressure. Here, $\phi(R, 0) = \frac{1}{2}(\cos \pi R + 1)$ if $R \leq 1$, $\phi(R, 0) = 0$ else and the dimensionless parameters $V_0 = 5$, $\Lambda = 10$, and $\beta = 100$. The inset shows the total number of A cells N_A normalized by its initial value $N_{A,0}$ as a function of T . Interfacial tension first suppresses the invading tissue, which eventually succeeds after the interface broadened.

$N_A = 2\pi\Omega_A^{-1} \int_0^\infty \phi r dr$, where we take Ω_A to be an effective two-dimensional cell volume, can be discussed using equation (15), which implies

$$\frac{dN_A}{dt} = \frac{2\pi}{\Omega_A} \int_0^\infty [-v_r \partial_r \phi + \kappa \Delta P^h \phi (1 - \phi)] r dr \quad (17)$$

(note that the diffusive term disappears under the integral). With equation (7), one eventually obtains

$$\frac{dN_A}{dt} = \frac{2\pi}{\Omega_A} \int_0^\infty \kappa \phi (P_A^h - P) r dr. \quad (18)$$

This equation shows that the number of A cells drops as long as $P > P_A^h$. If cell motion can be ignored, the typical pressure inside the region of A cells $P_A \simeq P_B^h + \Gamma/R$ has a contribution from the Laplace pressure Γ/R , where $\Gamma \simeq B/l$ is the surface tension (or line tension in two dimensions), l is the interface width, and R is the radius of the A-cell-rich region. We thus have

$$\frac{dN_A}{dt} \simeq N_A \kappa (\Delta P^h - \Gamma/R). \quad (19)$$

The suppression of A cells occurs if R is below a critical radius $R_c \simeq B/(\Delta P^h)$.

At long times, however, diffusion smears out the interface profile and l first increases as $l^2 \simeq Dt$ until it saturates at the finite value l_0 defined in equation (14). Therefore the surface tension drops and the critical radius becomes smaller. The stronger A cells with higher homeostatic pressure P^h can therefore possibly escape suppression and invade the weaker tissue with lower P^h even if initially the A-cell region is smaller than the critical radius.

This long-time growth of A cells into a region of B cells occurs only if the total number of A cells always remains larger than one. Note however that our continuum description with continuously varying cell volume fraction does not take the discrete character of cells into account. Therefore, this description misses the absorbing state when the last remaining A cell undergoes apoptosis. In this case, the continuum description breaks down and a more refined discrete description is needed.

If we apply this result to the situation of cancer invasion, these arguments therefore suggest that cell diffusion could increase significantly malignancy: when cancer cells become less cohesive and mix with cells of the host tissue, the tumor cannot be suppressed by interface tension only. If tumor and host tissue cannot freely mix (possibly separated by a physical barrier such as the basal membrane), the tumor can be suppressed if smaller than a critical radius R_c [4] and thus is statistically less dangerous.

5. Discussion

The interface dynamics discussed in this article is generic for tissues in which cells undergo cell division and apoptosis and interact. This is the case for developing tissues, where cell competition has been observed for example in the growing larva of *Drosophila* [18]; another example is the interface between a growing tumor and its surrounding host tissue. Using a continuum description, we find two regimes of interface propagation: a diffusive regime in which relative fluxes dominate the expansion (pulled front), and a propulsive regime in which the proliferation gives rise to convective flows (pushed front). In general, experiments will distinguish the regime in which a given system operates. Recent experiments focused on the growth dynamics of tumor cell spheroids that consist of one cell type only [5]. Taking a closer look at the combined growth dynamics of two cell populations will hopefully provide more insight into the different modes of homeostatic competition discussed in this article.

Here, we restricted our analysis to deterministic equations and noises are considered indirectly in the diffusion term. As cell division and cell death are stochastic events, it is straightforward to add a noise to the cell number balance. It is well known that in classical models for interface dynamics, noises can change the wave speed and the interface profile [19, 20]. We also discussed here only tissues with reduced dimensionality, assuming translational invariance along y or rotational symmetry, respectively. Additional insight into the dynamics in three dimensions may be gained from cell-based tissue simulations [21, 22].

References

- [1] Wolpert L 2005 *Principles of Development* 2nd edn (Oxford: Oxford University Press)
- [2] Weinberg R A 2006 *The Biology of Cancer* (New York: Garland Science)
- [3] Shraiman B I 2005 Mechanical feedback as a possible regulator of tissue growth *Proc. Natl Acad. Sci. USA* **102** 3318–23
- [4] Basan M, Risler T, Joanny J-F, Sastre-Garau X and Prost J 2009 Homeostatic competition drives tumor growth and metastasis nucleation *HFSP J.* **3** 265–72
- [5] Montel F *et al* 2011 Stress clamp experiments on multicellular tumor spheroids *Phys. Rev. Lett.* **107** 188102
- [6] Alberts B *et al* 2009 *Essential Cell Biology* 3rd edn (New York: Garland Science)

- [7] Ranft J, Basan M, Elgeti J, Joanny J-F, Prost J and Jülicher F 2010 Fluidization of tissues by cell division and apoptosis *Proc. Natl Acad. Sci. USA* **107** 20863–8
- [8] Fisher R A 1937 The wave of advance of advantageous genes *Ann. Hum. Genet.* **7** 355–69
- [9] Kolmogorov A, Petrovsky N and Piskounov N 1937 *Moscow Univ. Bull. Math.* **1** 1
Reprinted in Pelce P 1988 *Dynamics of Curved Fronts* (San Diego, CA: Academic) (Engl. transl.)
- [10] Pigolotti S, Benzi R, Jensen M H and Nelson D R 2012 Population genetics in compressible flows *Phys. Rev. Lett.* **108** 128102
- [11] Deroulers C, Aubert M, Badoual M and Grammaticos B 2009 Modeling tumor cell migration: from microscopic to macroscopic models *Phys. Rev. E* **79** 031917
- [12] Foty R A, Forgacs G, Pflieger C and Steinberg M S 1994 Liquid properties of embryonic tissues: Measurement of interfacial tensions *Phys. Rev. Lett.* **72** 2298–301
- [13] de Gennes P-G and Prost J 1993 *The Physics of Liquid Crystals* 2nd edn (Oxford: Clarendon Press)
- [14] Cochet-Escartin O, Ranft J, Silberzan P and Marcq P 2014 Border forces and friction control epithelial closure dynamics *Biophys. J.* **106** 65–73
- [15] Ranft J, Prost J, Jülicher F and Joanny J-F 2012 Tissue dynamics with permeation *Eur. Phys. J. E* **35** 46
- [16] Murray J D 1993 *Mathematical Biology* 2nd edn (New York, Heidelberg: Springer)
- [17] van Saarloos W 2003 Front propagation into unstable states *Phys. Rep.* **386** 29–222
- [18] Baker N E 2011 Cell competition *Curr. Biol.* **21** R11–5
- [19] Brunet E and Derrida B 1997 Shift in the velocity of a front due to a cutoff *Phys. Rev. E* **56** 2597–604
- [20] Hallatschek O and Korolev K 2009 Fisher waves in the strong noise limit *Phys. Rev. Lett.* **103** 108103
- [21] Basan M, Prost J, Joanny J-F and Elgeti J 2011 Dissipative particle dynamics simulations for biological tissues: rheology and competition *Phys. Biol.* **8** 026014
- [22] Drasdo D and Hoehme S 2012 Modeling the impact of granular embedding media, and pulling versus pushing cells on growing cell clones *New J. Phys.* **14** 055025